Porous Materials Hot Paper

How to cite: Angew. Chem. Int. Ed. 2021, 60, 10902–10909
International Edition: doi.org/10.1002/anie.202100240
German Edition: doi.org/10.1002/ange.202100240

Amino-Functionalised Hybrid Ultramicroporous Materials that Enable Single-Step Ethylene Purification from a Ternary Mixture

Soumya Mukherjee[+], Naveen Kumar[+], Andrey A. Bezrukov, Kui Tan, Tony Pham, Katherine A. Forrest, Kolade A. Oyekan, Omid T. Qazvini, David G. Madden, Brian Space, and Michael J. Zaworotko**

Abstract: *Pyrazine-linked hybrid ultramicroporous (pore size < 7 Å) materials (HUMs) offer benchmark performance for trace carbon capture thanks to strong selectivity for CO_2 over small gas molecules, including light hydrocarbons. That the prototypal pyrazine-linked HUMs are amenable to crystal engineering has enabled second generation HUMs to supersede the performance of the parent HUM,* ***SIFSIX-3-Zn****, mainly through substitution of the metal and/or the inorganic pillar. Herein, we report that two isostructural aminopyrazine-linked HUMs,* ***MFSIX-17-Ni*** *(17 = aminopyrazine; M = Si, Ti), which we had anticipated would offer even stronger affinity for CO_2 than their pyrazine analogs, unexpectedly exhibit reduced CO_2 affinity but enhanced C_2H_2 affinity.* ***MFSIX-17-Ni*** *are consequently the first physisorbents that enable single-step production of polymer-grade ethylene (> 99.95 % for* ***SIFSIX-17-Ni****) from a ternary equimolar mixture of ethylene, acetylene and CO_2 thanks to coadsorption of the latter two gases. We attribute this performance to the very different binding sites in* ***MFSIX-17-Ni*** *versus* ***SIFSIX-3-Zn****.*

Introduction

The chemical industry accounts for around 7 % of World GDP with revenue of $5.7 trillion/annum.[1] Its energy footprint, which is driven by downstream purification of commodity chemicals, is even larger, representing ca. 15 % of global energy consumption.[2] Overall, separation/purification of commodity chemicals alone represents ca. 40 % of the industrially consumed energy.[3] Forecasts have indicated that by 2050 there will be a three-fold increase in demand for commodity chemicals, demanding more energy-efficient approaches to commodity purification.[3] As the basic feedstock for the production of plastics, detergents and coatings, ethylene (C_2H_4) is the highest volume product of the global chemical industry.[4] The production of C_2H_4 and propylene alone account for 0.3 % of global energy.[5] The energy-intensive state-of-the-art for production of polymer-grade (> 99.95 % purity) C_2H_4 involves steam cracking of hydrocarbons.[5,6] Alternatively, oxidative coupling of methane (CH_4) results in gas mixtures that include acetylene (C_2H_2) and carbon dioxide (CO_2) in addition to C_2H_4.[7] Production of polymer-grade C_2H_4 therefore involves removal of these two impurities from $C_2H_4/C_2H_2/CO_2$ ternary mixtures. Presently, C_2H_2 is removed via one of two processes: catalytic hydrogenation (using expensive noble-metal catalysts at high temperature/pressure); solvent extraction (causing solvent waste with the need for large operating units). CO_2 is also removed chemically, using caustic soda.[5] Physisorbents offer potential to greatly reduce the energy footprint of separation processes.[3,8] Nevertheless, despite advances in gas purification from binary mixtures using physisorbents under ambient pressure and temperature,[9] including C_2H_4,[10] C_2H_4 purification from ternary C2-CO_2 mixtures remains an unmet challenge.[11] This is largely a consequence of the similar physicochemical properties (molecular sizes and boiling points, Scheme S1) of the three components[11a,12] and the absence of physisorbents that selectively exclude C_2H_4. One approach to address this challenge is the use of multiple ultramicroporous physisorbents using synergistic sorbent separation technology, SSST.[13] Another approach would be

[*] Dr. S. Mukherjee,[+] N. Kumar,[+] Dr. A. A. Bezrukov, Dr. D. G. Madden, Prof. M. J. Zaworotko
Bernal Institute, Department of Chemical Sciences
University of Limerick
Limerick V94 T9PX (Ireland)
E-mail: xtal@ul.ie

Dr. S. Mukherjee[+]
Department of Chemistry, Technical University of Munich
Lichtenbergstraße 4, 85748 Garching b. München (Germany)
E-mail: soumya.mukherjee@tum.de

Dr. K. Tan, K. A. Oyekan
Department of Materials Science & Engineering
University of Texas at Dallas
Richardson, TX 75080 (USA)

Dr. T. Pham, Dr. K. A. Forrest, Prof. B. Space
Department of Chemistry, University of South Florida
4202 East Fowler Avenue, CHE205, Tampa, FL 33620-5250 (USA)

Dr. O. T. Qazvini
Department of Chemical Engineering and Analytical Science
The University of Manchester
Oxford Road, Manchester M13 9PL (UK)

Prof. B. Space
Department of Chemistry, North Carolina State University (USA)

[+] These authors contributed equally to this work.

Supporting information and the ORCID identification number(s) for the author(s) of this article can be found under: https://doi.org/10.1002/anie.202100240.

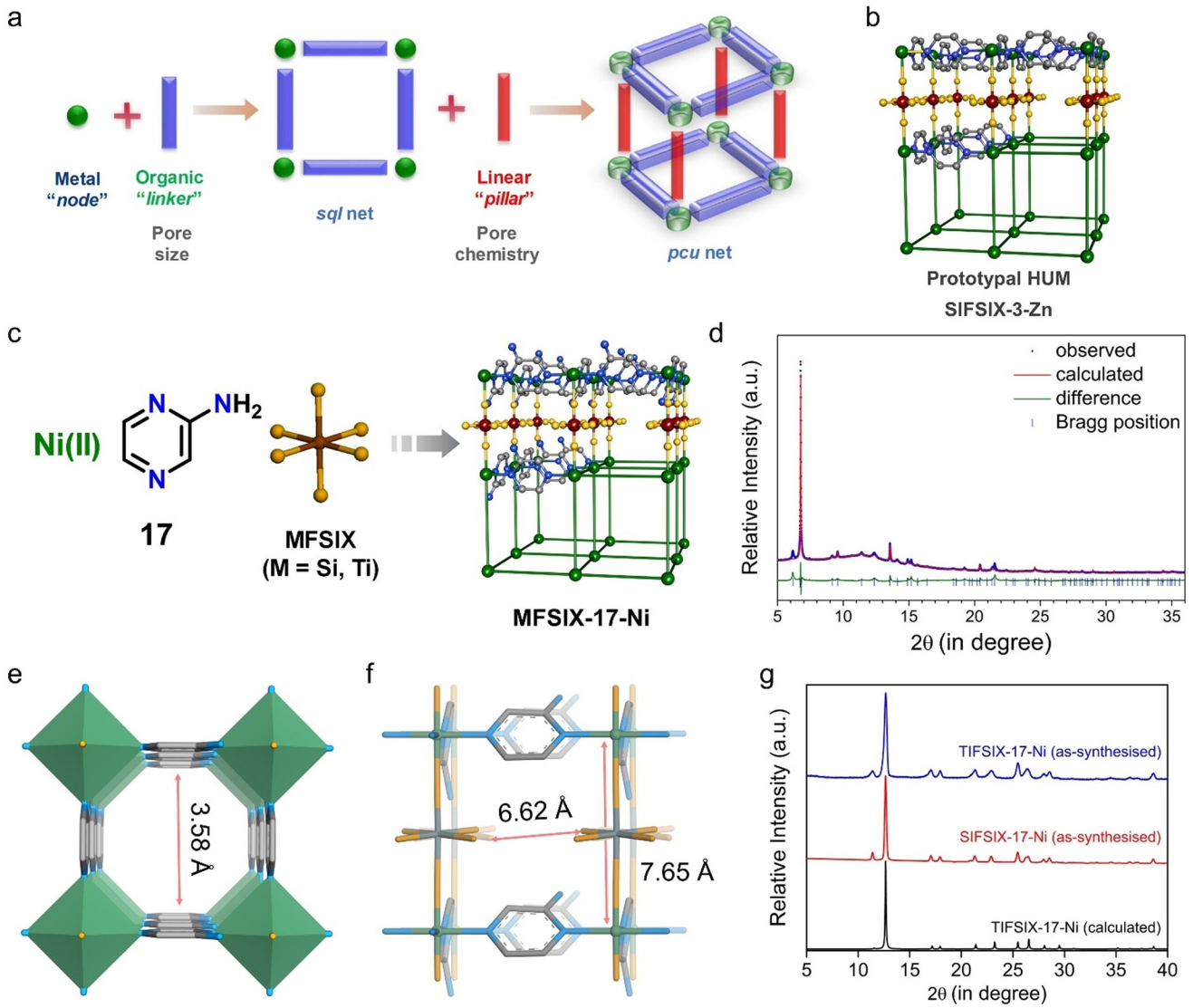

Figure 1. a) Schematic illustration of the modularity of pillared square grids that form **pcu** topology HUMs, enabling exquisite control of both pore size and pore chemistry. b) The prototypal pyrazine (pyz) linked HUM $[Zn(pyz)_2(SiF_6)]_n$, **SIFSIX-3-Zn**, is formed from Zn^{II}-pyz cationic **sql** nets and inorganic SiF_6^{2-} (SIFSIX) pillars. c) Schematic illustration of the building blocks (Ni^{II}, pyz-NH_2 linker ligand (**17**), SIFSIX/TIFSIX inorganic pillars) and the **pcu** network topology of **MFSIX-17-Ni**. d) Rietveld refinement plot for desolvated **TIFSIX-17-Ni** (dynamic vacuum, 298 K), Rwp = 4.69 %. Powder X-ray diffraction, PXRD, data was collected using synchrotron radiation, $\lambda = 0.82455(2)$ Å. e) Cross-sectional channel view of the desolvated crystal structure of **TIFSIX-17-Ni** along the crystallographic *c* axis; 3.59 × 3.59 Å ultramicropores are formed. f) Crystal structure of desolvated **TIFSIX-17-Ni** viewed along the *a*- and *b*-axes; Ni^{II}-NH_2-pyz **sql** layers are pillared by TiF_6^{2-} anions. g) Comparison of as-synthesised PXRD patterns (CuKα radiation, $\lambda\alpha = 1.54056$ Å) of the **MFSIX-17-Ni** phases with the calculated pattern of **TIFSIX-17-Ni**. Colour codes: grey, C; blue, N; red, O; orange, F; green (polyhedra and spheres in Figures 1e and 1f, respectively), Ni; greenish grey, Ti.

to exploit a single sorbent[14] that is highly selective for both CO_2 and C_2H_2 over C_2H_4 under ambient conditions, the first example of which is reported herein.

Metal–organic materials (MOMs),[15] including metal–organic frameworks (MOFs)[16] and hybrid ultramicroporous materials (HUMs),[17] are attractive candidates for sorbent design since they are modular.[18] HUMs, which can generally be described as 2D square lattice (**sql**) metal–organic networks pillared by inorganic anions (e.g. SiF_6^{2-}, TiF_6^{2-}, $NbOF_5^{2-}$) with **pcu** topology (Figure 1a), can combine the right pore chemistry (strong electrostatics) and pore size (high density of tight binding sites). The resulting energetic "*sweet spots*" have enabled HUMs to be the current selectivity benchmarks for several industrially relevant binary gas separations, including C_2H_2 over C_2H_4 (S_{AE})[19] and CO_2 over N_2 (S_{CN}).[20] Unfortunately, these benchmark HUMs are unsuited for ternary C2-CO_2 separations because, whereas they are highly selective for one of the two impurities over C_2H_4, they are not selective enough to address the other impurity. Herein, we report on the unexpected outcome of our study on the sorption properties of an amine functionalised variant of the **SIFSIX-3-Zn** (Figure 1b) family of HUMs,[20a] **MFSIX-17-Ni** (M = Si, Ti; **17** = pyz-NH_2 = 2-aminopyrazine).

Results and Discussion

Solvothermal reaction of pyz-NH_2 with nickel hexafluorotitanate afforded the previously unreported HUM, $[Ni(pyz\text{-}NH_2)_2(TiF_6)]_n$, **TIFSIX-17-Ni** (Figures 1 c, S1), as a dark green microcrystalline powder. **TIFSIX-17-Ni** is an analogue of the previously reported sorbent **ZJUT-1** (ZJUT = Zhejiang University of Technology).[21] **ZJUT-1** (termed **SIFSIX-17-Ni** herein) was reported in 2018 and studied in the context of propyne/propylene separation but remains unexplored with respect to C2 and CO_2 gas sorption. The structure of desolvated **TIFSIX-17-Ni** was determined from in situ synchrotron powder X-ray diffraction (PXRD) data obtained from beamline i11[22] at the Diamond Light Source at 298 K (Figure 1 d, see Supporting Information Table S1 for details). **TIFSIX-17-Ni** has the same **pcu** network connectivity and is isostructural with its pyz based analogue, $[Ni(pyz)_2(SiF_6)]_n$, **SIFSIX-3-Ni**.[20b,23] The *c* distance is slightly greater in **TIFSIX-17-Ni** (Figure S6) than **SIFSIX-3-Ni** ($\approx$7.65 Å versus $\approx$7.5 Å, respectively) (Figures 1 f, S7). The *a* distances, 6.98 Å (**TIFSIX-17-Ni**) versus 7.01 Å (**SIFSIX-3-Ni**), are comparable. The pore shape/chemistry, however, is profoundly affected by the amino group in **TIFSIX-17-Ni**. Specifically, axial F atoms in SiF_6^{2-} orient towards the pore at 45° to the crystallographic *a* axis in desolvated **SIFSIX-3-Ni**, whereas the F atoms in desolvated **TIFSIX-17-Ni** orient at 35°, meaning that pyz rings are disordered between two positions and amino groups are disordered over four positions (Figure S8). This structural difference can be attributed to F···NH_2 H-bonding interactions and, as discussed below, importantly results in a longer F···F diagonal distance across the pore (Figure 1 f; Figures S7, S8). After confirming bulk phase purity (Figure 1 g; Figures S2, S3), thermogravimetric analysis (TGA) profiles (Figure S9) indicated that activated **SIFSIX-17-Ni** and **TIFSIX-17-Ni** are stable to 493 K and 533 K respectively. In situ synchrotron PXRD experiments confirmed rigidity of the frameworks upon desolvation; only minor decreases in unit cell volumes of 2.9 % and 1.8 % were observed for **SIFSIX-17-Ni** and **TIFSIX-17-Ni**, respectively (Figures S4, S5). Contraction mainly occurred along the *c* axis: 2.0 % along *c* versus 0.4 % along *a* for **SIFSIX-17-Ni**; 1.2 % along *c* versus. 0.3 % along *a* for **TIFSIX-17-Ni**. The stability of **MFSIX-17-Ni** to humidity was confirmed using an accelerated stability protocol adopted by the pharmaceutical industry (test at 313 K and 75 % RH) (Figures S10–S12).[24]

The sorption properties of **MFSIX-17-Ni** were first examined using single-component isotherms (Figures S13–S26). Type I cryogenic (195 K) CO_2 isotherms (Figures S13, S14) for both pyz-NH_2 HUMs revealed Brunauer-Emmett-Teller (BET) surface areas of 229.2 (**SIFSIX-17-Ni**) and 237.6 $m^2 g^{-1}$ (**TIFSIX-17-Ni**). The 298 K and 273 K isotherms indicated affinity for sorbates as follows: CO_2 over nitrogen (N_2) and CH_4; C_2H_2 over C_2H_4 and ethane (C_2H_6) (Figures S15–S22). These affinities contrast to the isostructural pyz linked HUMs, **MFSIX-3-Ni**. Specifically, amine introduction resulted in enhanced C_2H_2 affinity and, unexpectedly given the presence of amino groups, reduced CO_2 affinity (Figures 2 a,b). These trends are most pronounced in the low pressure region (< 10 000 ppm or 0.01 bar) which is so critical for trace separations. Uptakes at 0.01 bar (mmol g^{-1}) for CO_2 were as follows: **SIFSIX-17-Ni** (0.20) < **TIFSIX-17-Ni** (0.32) < **SIFSIX-3-Ni** (1.76) < **TIFSIX-3-Ni** (2.16). The corresponding trend for C_2H_2 was **SIFSIX-3-Ni** (0.29) < **TIFSIX-3-Ni** (0.55) < **SIFSIX-17-Ni** (0.91) < **TIFSIX-17-Ni** (1.38).

Low-coverage isosteric enthalpy of adsorption (Q_{st}) values were determined from the CO_2 and C_2H_2 adsorption isotherms recorded at 273 and 298 K (Figures S23–S26) by fitting them to a virial-type expression (methods section, Supporting Information; Figures S27–S30 and Tables S4–S7). **MFSIX-3-Ni** was found to exhibit higher $Q_{st}(CO_2)$ values at low loading than the **MFSIX-17-Ni** HUMs: **TIFSIX-17-Ni** (37.8 kJ mol^{-1}) < **SIFSIX-17-Ni** (40.2 kJ mol^{-1}) < **SIFSIX-3-Ni** (44.4 kJ mol^{-1}) < **TIFSIX-3-Ni** (49.5 kJ mol^{-1}). The reverse trend was observed for $Q_{st}(C_2H_2)$: **TIFSIX-3-Ni** (38.8 kJ mol^{-1}) < **SIFSIX-3-Ni** (37.0 kJ mol^{-1}) < **SIFSIX-17-Ni** (44.2 kJ mol^{-1}) < **TIFSIX-17-Ni** (48.3 kJ mol^{-1}). The Q_{st} values were determined to be consistent across CO_2 and C_2H_2 loading. This is supported by the rigid nature of both pyz-NH_2 HUMs as evident from in situ PXRD analyses (Figures S4, S5). These studies suggest single site CO_2/C_2H_2 binding in **MFSIX-17-Ni**. Ideal adsorbed solution theory, IAST[25] selectivities were calculated by fitting the single-component C_2H_2, CO_2 and C_2H_4 isotherms to the dual-site Langmuir–Freundlich DSLF equation (see Supporting Information for details, Table S8) for binary gas mixtures of C_2H_2/C_2H_4 and C_2H_2/CO_2 (both 1:1, *v*/*v*) at 1 bar and 298 K. High C_2H_2/C_2H_4 selectivities (S_{AE}) were obtained for both **SIFSIX-17-Ni** (506.4) and **TIFSIX-17-Ni** (670.9) (Figure S31, values in parenthesis denote S_{AE} at 1 bar and 298 K). Figure 2 e reveals C_2H_2/CO_2 selectivities (S_{AC}) for **SIFSIX-17-Ni** and **TIFSIX-17-Ni** of 11.7 and 20.9, respectively, at 1 bar and 298 K, whereas CO_2/C_2H_2 selectivities (S_{CA}) for **SIFSIX-3-Ni** and **TIFSIX-3-Ni** of 6.6 and 17.6, respectively, were determined. To our knowledge, this is only the second occurrence of "inverted" C_2H_2 versus CO_2 sorption within a family of physisorbents.[26]

The similarity in $Q_{st}(CO_2)$ and $Q_{st}(C_2H_2)$ values for **MFSIX-17-Ni** HUMs implies that coadsorption of CO_2 and C_2H_2 could occur under dynamic conditions such as dynamic column breakthrough (DCB) experiments. Ambient temperature (298 K) and pressure (1 bar) DCB experiments were conducted using fixed-bed columns of each of the four HUM adsorbents with three inlet gas mixtures of fixed composition (*v*/*v*): two binary mixtures, C_2H_4/C_2H_2 (1:1), CO_2/C_2H_2 (1:1); one ternary mixture $C_2H_4/C_2H_2/CO_2$ (1:1:1) (Figures 2 g, h; Figures S32–S34; for experimental details, see Supporting Information). For the **MFSIX-3-Ni** HUMs, the respective breakthrough times confirmed effective separation for each of the three gas mixtures (Figures S32, S34) with C_2H_2 eluting last in each case except for the CO_2/C_2H_2 (1:1) DCB experiment with **TIFSIX-3-Ni** (Figure S32d), for which coadsorption resulted in no separation. For the **MFSIX-17-Ni** HUMs, each DCB experiment was successful in terms of separating the three gas mixtures by eluting pure C_2H_4 or CO_2 as the effluent (Figures 2 g, h; Figure S33). Unlike the **MFSIX-3-Ni** HUMs, which suffer from C_2H_4/C_2H_2 coadsorption (Figure S32),[26] the binary C_2H_4/C_2H_2 DCB experiments with **MFSIX-17-Ni** HUMs led to negligible C_2H_4 uptakes (Figure S33) and elution of high-purity (> 99.95 %) C_2H_4 for

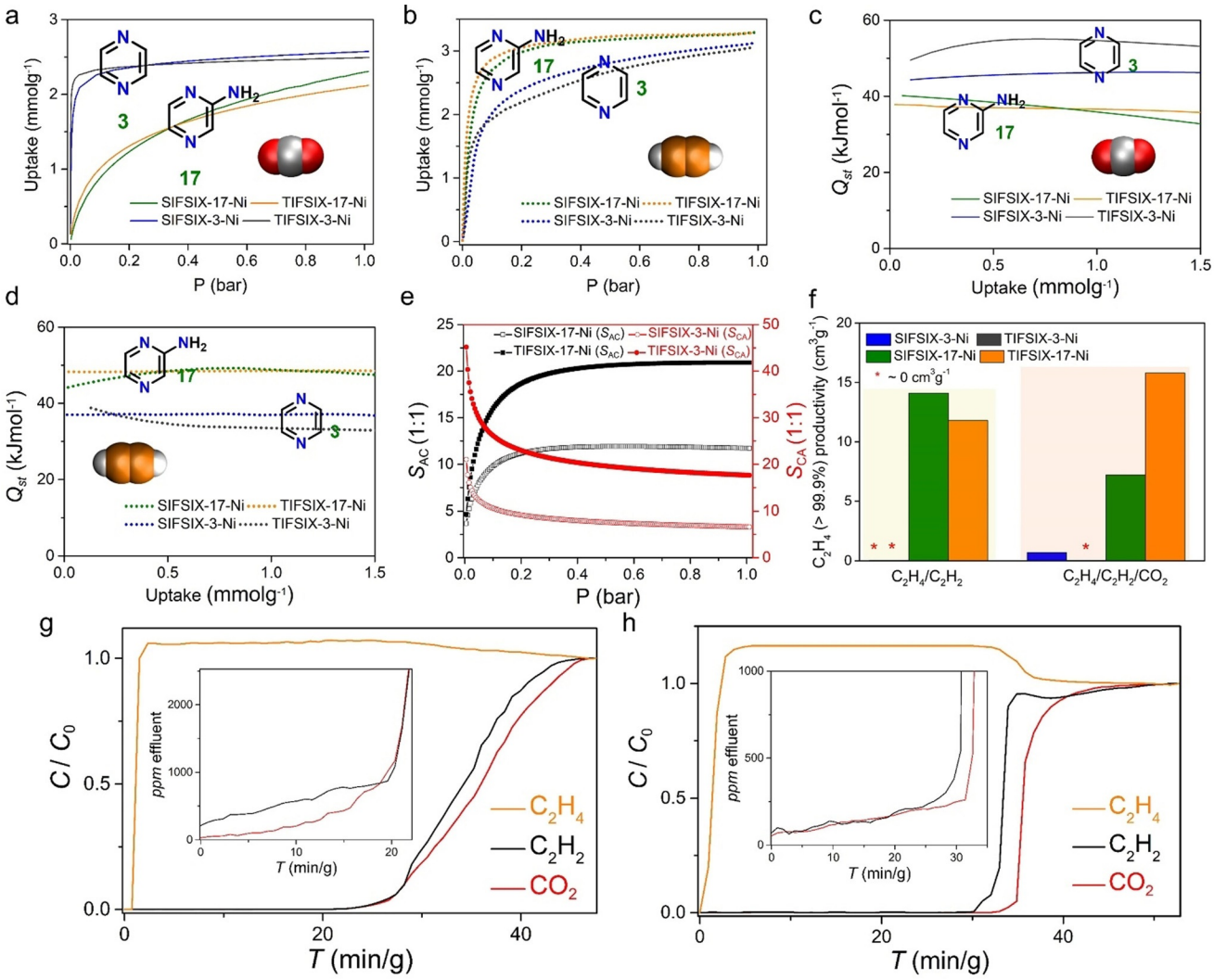

Figure 2. a) CO_2 and b) C_2H_2 sorption isotherms at 298 K for **MFSIX-3-Ni** and **MFSIX-17-Ni**; the isosteric enthalpies of adsorption for c) CO_2 and d) C_2H_2 for **MFSIX-3-Ni** and **MFSIX-17-Ni**. e) Ideal adsorbed solution theory, IAST selectivity (at 298 K until 1 bar) trends for C_2H_2 over CO_2, S_{AC} and for CO_2 over C_2H_2, S_{CA} (1:1, v/v gas mixtures). f) Dynamic column breakthrough, DCB experiments derived comparison of high-grade (99.9%) C_2H_4 productivity ($cm^3 g^{-1}$) for binary C_2H_4/C_2H_2 and ternary $C_2H_4/C_2H_2/CO_2$ (volumetric ratios of 1:1 and 1:1:1, respectively) mixtures. Ambient temperature (298 K) and pressure (1 bar) experimental DCB curves for $C_2H_4/C_2H_2/CO_2$ (1:1:1, v/v) ratio by a sorbent bed filled with g) **SIFSIX-17-Ni** and h) **TIFSIX-17-Ni** (total gas flow: 2.1 $cm^3 min^{-1}$). Insets of (g) and (h) present the C_2H_2 and CO_2 effluent concentrations for **SIFSIX-17-Ni** and **TIFSIX-17-Ni**, respectively in the above-mentioned DCB experiments.

a relatively long time as supported by monitoring of C_2H_4 effluent purity levels during DCB experiments (Table S9). Perhaps our most significant observations concern the ternary $C_2H_4/C_2H_2/CO_2$ (1:1:1) breakthrough experiments (Figures 2 g, h; Figure S34). Whereas **MFSIX-3-Ni** separated the C2-CO_2 stream, coadsorption of CO_2 and C_2H_2 was found to occur only for a relatively short duration before CO_2 adsorption dominated. The breakthrough sequence was C_2H_4 (1/1 min g^{-1}) < C_2H_2 (20/22.5 min g^{-1}) < CO_2 (32/32 min g^{-1}) for the **SIFSIX-3-Ni/TIFSIX-3-Ni** packed sorbent beds (Figure S34). This resulted in low ethylene productivity and compromised ethylene purity in the effluent stream (Figure 2 f; Table S9). Conversely, for the **MFSIX-17-Ni** sorbent beds, the breakthrough sequence was C_2H_4 (0.7/0.5 min g^{-1}) < C_2H_2 (25/30 min g^{-1}) < CO_2 (25.8/32 min g^{-1}) for **SIFSIX-17-Ni/TIFSIX-17-Ni**, respectively (Figures 2 g,h). C_2H_4 effluent streams from the **SIFSIX-17-Ni** and **TIFSIX-17-Ni** fixed beds revealed C_2H_4 purity as high as 99.958% and 99.912% with high-purity ethylene productivities of 7.2 and 15.8 $cm^3 g^{-1}$, respectively (Figure 2 f; Table S9). We attribute the similar elution times of CO_2 and C_2H_2 to coadsorption driven by the similar affinities for these sorbents when exposed to C2-CO_2 ternary mixtures.

In situ infrared (IR) spectroscopy was employed to elucidate the mechanism of the sorbent-sorbate interactions. **TIFSIX-3-Ni** and **TIFSIX-17-Ni** were first heated in high vacuum for activation and then cooled to room temperature for recording the IR spectra of activated samples and to monitor the loading of CO_2 and C_2H_2 (Figure 3). We first established the assignment of HUM vibrational bands by comparing with the reported spectrum of matrix isolated (monomeric) pyz,[27] and through density functional theory

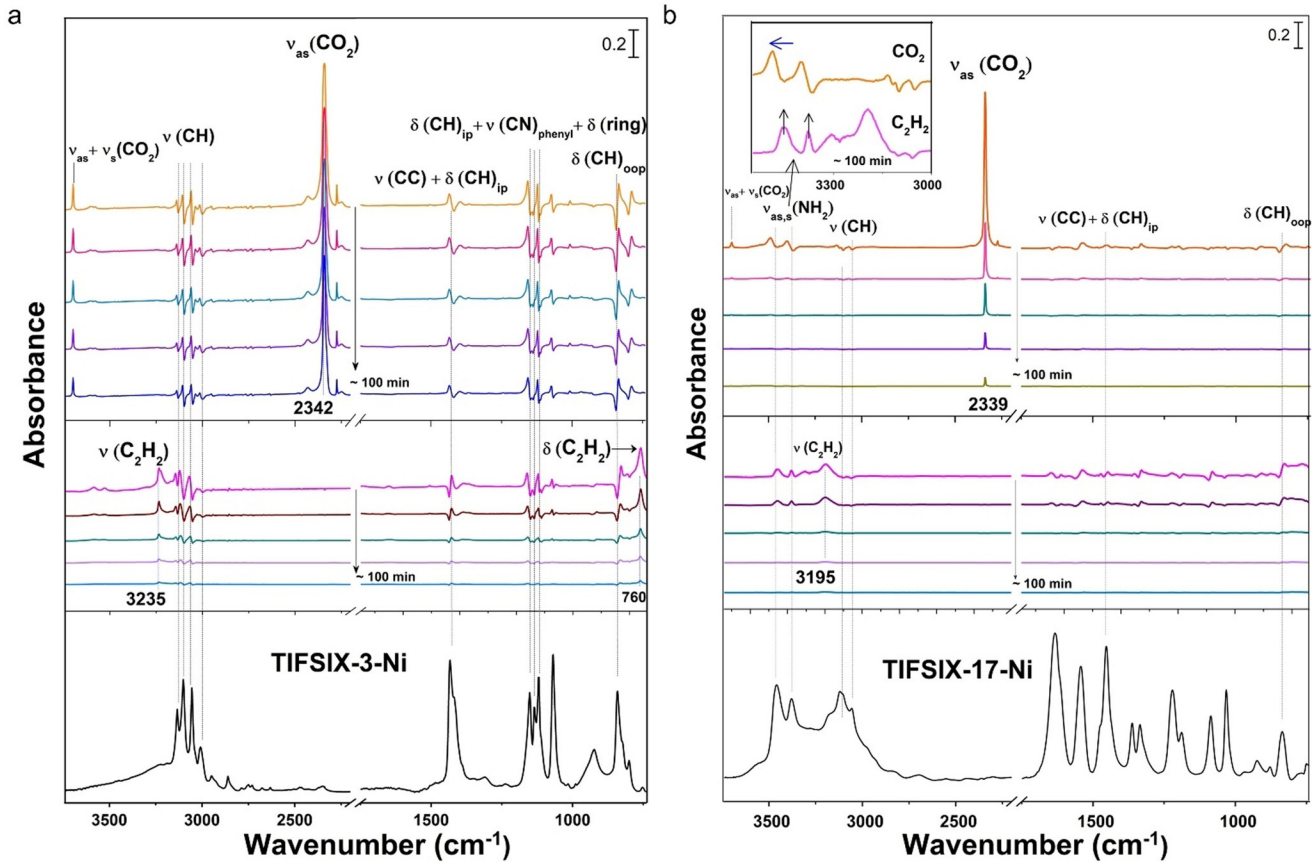

Figure 3. IR spectra showing adsorbed CO_2 and C_2H_2 in **TIFSIX-3-Ni** (a) and **TIFSIX-17-Ni** (b), respectively. Top and middle panels: difference spectra of unloading CO_2 (top) and C_2H_2 (middle) process from two HUMs under vacuum, each spectrum is referenced to the spectra of activated **TIFSIX-3-Ni** and **TIFSIX-17-Ni** sample. The orange and pink spectra are recorded after subsequent evacuation of ≈1 bar gas phase CO_2 and C_2H_2 within ≈5 s. Bottom panel: IR spectra of activated **TIFSIX-3-Ni** and **TIFSIX-17-Ni**, referenced to pure KBr pellet in vacuum (<0.027 mbar base pressure).

(DFT) calculations on the vibrational frequency of pyz-NH_2 linker. Table S10 summarises the detailed assignment of observed bands in Figure 3. 1 bar CO_2 was then introduced into the activated samples for ≈5 min to ensure adsorption saturation. We note that the IR absorption of gas phase CO_2 is prohibitively high at this pressure, precluding the observation of adsorbed CO_2. We then evacuated the chamber and recorded spectra as a function of time during desorption. Within ≈5 seconds of evacuation, the pressure of gas-phase CO_2 drops below ≈0.7 mbar (negligible gas-phase IR absorption). The adsorbed CO_2 within **TIFSIX-3-Ni** is initially detected by its characteristic peak at 2342 and 3699 cm^{-1} in the difference spectra of Figure 3a, which corresponds to the asymmetric stretching band $\nu_{as}(CO_2)$ and combination band $\nu_a+\nu_s$ (CO_2).[28] The desorption of CO_2 from **TIFSIX-3-Ni** was relatively slow, intensity of the $\nu_{as}(CO_2)$ band decreasing by only ≈35% after ≈100 min of evacuation at room temperature (Figure S35). This is in agreement with the pure CO_2 isotherm based strong binding of CO_2 to **TIFSIX-3-Ni**.[29] The peak width of $\nu_{as}(CO_2)$ band, determined by Voigt profile fitting, is 7.7 cm^{-1} and the initial $\nu_{as}(CO_2)$ spectrum in **TIFSIX-3-Ni** exhibits an asymmetric line shape (Figure S36). Desorption of CO_2 is facilitated upon heating the sample to 423 K for ≈20 min in vacuum. After evacuation of most of the adsorbed CO_2 molecules from **TIFSIX-3-Ni** (Figure S36), the remaining $\nu_{as}(CO_2)$ band narrows and red-shifts to 2339 cm^{-1}, the same position as the adsorbed CO_2 in **TIFSIX-17-Ni**. Meanwhile, the spectral line becomes more symmetric. The broadening and asymmetric line shape of the $\nu_{as}(CO_2)$ band in **TIFSIX-3-Ni** suggests strong vibrational dynamic coupling between adsorbed CO_2 molecules and the pyz-linked ultramicropores under high loading.[30] Our previous reports on **MFSIX-3-Ni** have identified binding sites via molecular modelling[26] and PXRD derived structural solution.[23] These studies revealed that CO_2 interacts primarily with four electronegative F atoms from surrounding SiF_6^{2-} anions and are key to its benchmark CO_2 selectivity.[20b] However, the interactions between CO_2 and TiF_6^{2-} anions in **TIFSIX-3-Ni** and **TIFSIX-17-Ni** cannot be directly characterised by IR spectroscopy since the vibrations of TiF_6^{2-} occur below 650 cm^{-1}, beyond the detection range of an infrared MCT-A detector. Nevertheless, difference spectra offer additional evidence that CO_2 interacts with the pyz linker in **TIFSIX-3-Ni**, as suggested by the strong perturbation of characteristic bands including ν(CH), $\nu(CC)_{phenyl}$, $\delta(CH)_{ip}$ and δ $(CH)_{oop}$. In comparison with **TIFSIX-3-Ni**, the spectra for **TIFSIX-17-Ni** exhibit marked differences in both CO_2 and perturbed phenyl ring bands. For $\nu_{as}(CO_2)$ band at 2139 cm^{-1} in **TIFSIX-17-Ni**,

its peak width is 5.5 cm^{-1}, narrower compared to that in **TIFSIX-3-Ni**. The band decreases quickly upon evacuation and within ≈100 min only <5% of its initial intensity remained (Figure S35). A fast reduction of the combination band $\nu_{as}+\nu_{s,}$ at 3696 cm^{-1} is also evident in Figure 3b. Perturbation of the phenyl ring bands is also much weaker compared to **TIFSIX-3-Ni**, thus supporting the sorption experiments which indicate that introduction of the NH_2 group reduces CO_2 affinity in **TIFSIX-17-Ni**. This behaviour can be attributed to two effects. First, the presence of NH_2 within the channel isolates the adsorbed CO_2 molecules and prevents their dynamic coupling as indicated by the narrowing of $\nu_{as}(CO_2)$ band in **TIFSIX-17-Ni**. Secondly, CO_2 interactions with pyz cause the degree of phenyl ring modes' perturbation to decrease when the hydrogen atoms of the pyz linker are substituted by -NH_2. Chemisorption driven carbamate formation,[31] as encountered in amine-grafted physisorbents, did not occur according to the difference spectra for **TIFSIX-17-Ni** in the region 1000–1800 cm^{-1}. No peaks associated with the ν(C=O), ν(C-N) bands of carbamate were observed.[32] Furthermore, we found that the ν(N-H) bands exhibited an unusual blue shift upon loading of CO_2. This observation suggests that adsorbed CO_2 molecules did not form H-bonding interactions with the -NH_2 group, which would have shifted the ν(N-H) frequency downwards.[33] Rather, this result is indicative that the N–H bond is strengthened by encountering a repulsive force from the adsorbed CO_2.

The samples were in situ regenerated in vacuum at 383 K and cooled back to 298 K for the corresponding C_2H_2 experiments. Upon adsorbing C_2H_2, the perturbations of phenyl modes behaved similarly to CO_2 loading, i.e., they are more significant in **TIFSIX-3-Ni** than in **TIFSIX-17-Ni**. However, we noted that the ν(N-H) bands respond differently from loading of CO_2. The two ν(N-H) bands increase in intensity upon increased dosing of C_2H_2 (Inset, Figure 3b). The intensity of ν(N-H) bands is usually correlated with the basicity of the amine group. As the basicity decreases when -NH_2 bind with an acidic group, the ν(N-H) bands grow stronger.[34] C_2H_2 is well-known to show acidity and can form HC≡CH···N complexes through strong hydrogen bonding according to ab initio calculations.[35] It was determined by GCMC simulations that the C_2H_2 binding site in **SIFSIX-3-Ni** involves multiple C–H···F interactions.[13] We infer that the adsorbed C_2H_2 forms C–H···N hydrogen bonds with -NH_2 in **TIFSIX-17-Ni**. This is supported by the observation that the stretching band ν(C–H) of adsorbed C_2H_2 within **TIFSIX-17-Ni** appears at a lower frequency of 3195 cm^{-1} and displays broader line-shape when compared with the corresponding peak in **TIFSIX-3-Ni**.

Insights into the nature of the binding sites for C_2H_2, CO_2, and C_2H_4 in **TIFSIX-17-Ni** were revealed through classical molecular simulations (for full details, see Supporting Information). Figures 4d, e and f show a comparison of the modelled binding sites for each adsorbate in **TIFSIX-17-Ni** versus those in **SIFSIX-3-Ni** (Figures 4a, b and c).[13] It was observed that all three molecules are oriented vertically along

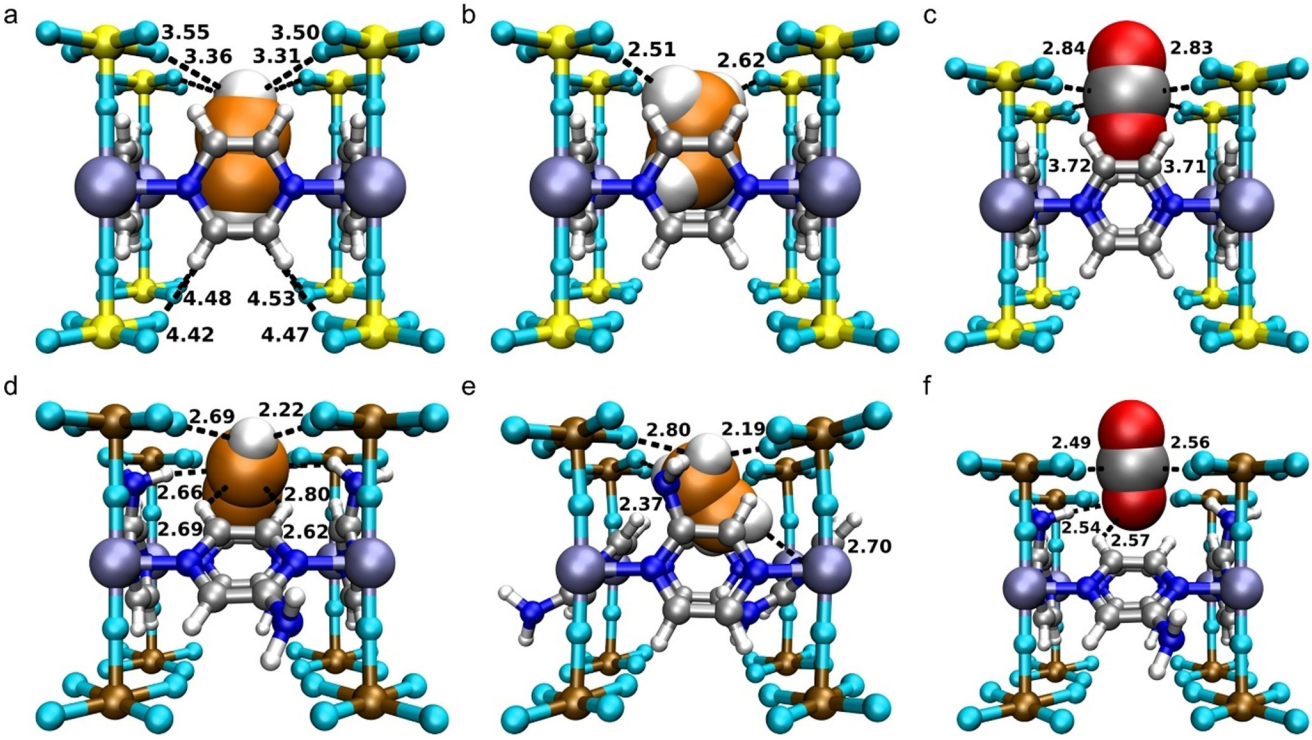

Figure 4. C_2H_2 (a, d), C_2H_4 (b, e) and CO_2 (c, f) binding sites in **SIFSIX-3-Ni** (top) and **TIFSIX-17-Ni** (bottom). Closest contacts between HUM atoms and the gas molecules are defined by the distances (in Å) between the H atom of hydrocarbons and the closest framework atoms. Adsorbed C2 and CO_2 molecules are presented in space-filling mode (C, grey; H, white; O, red; N, blue; F, cyan; Si, yellow; Ni, lavender; Ti, gold).

the *c*-axis in the channels of **SIFSIX-3-Ni**, where they interact with equatorial F atoms of the SiF_6^{2-} groups. On the other hand, the tilt of the pyz rings, longer F···F diagonal distance across the unit cell, and presence of the -NH_2 groups on the linkers in **TIFSIX-17-Ni** cause the C_2H_2 molecules to align within the pores at an angle with respect to the square grid. This results in shorter H···F interactions between the C_2H_2 and the inorganic pillars compared to those in **SIFSIX-3-Ni**. The C_2H_2 molecules also interact favourably with the -NH_2 groups on the linkers as it is adsorbed near the TiF_6^{2-} pillars. Both types of HUM-adsorbate interactions contribute to a high calculated binding energy for C_2H_2 in **TIFSIX-17-Ni**, especially compared to that in **SIFSIX-3-Ni**.

C_2H_4 exhibits a similar orientation within the channels of **TIFSIX-17-Ni** to that of C_2H_2 but makes fewer contacts with the framework, resulting in lower affinity and selectivity for C_2H_4. The calculated binding energy for C_2H_4 in **TIFSIX-17-Ni** was determined to be lower than both C_2H_2 and CO_2, consistent with the results obtained for **SIFSIX-3-Ni**.[13] The orientation of CO_2 molecules around the TiF_6^{2-} pillars in **TIFSIX-17-Ni** is similar to that observed in **SIFSIX-3-Ni** as well as to other members of the **SIFSIX-3-M** series.[20a,23,36] However, the CO_2 molecule exhibits O···N repulsion with the surrounding -NH_2 groups on the linker, thereby decreasing its interaction energy relative to that of **SIFSIX-3-Ni**. The trend in the calculated binding energy for the different adsorbates localised in **TIFSIX-17-Ni** is $C_2H_2 > CO_2 > C_2H_4$ (see Supporting Information, Figures S38–40), which is consistent with the trend in the experimental low-coverage Q_{st} values.

Conclusion

MFSIX-17-Ni are the first physisorbents that enable single-step production of polymer-grade (> 99.95 %) ethylene from a ternary equimolar mixture of ethylene, acetylene and CO_2 under ambient conditions. We attribute these results to the binding sites in **MFSIX-17-Ni**, which are very different to those in the isostructural family of HUMs based upon **SIFSIX-3-Zn**. These binding sites are impacted by the presence of amino groups and enable coadsorption of CO_2 and C_2H_2, thanks to high affinity towards both gases. This study once again illustrates how apparently subtle changes in pore size,[37] shape[38] and chemistry[39] in ultramicroporous materials can profoundly impact selectivity and separation performances,[11a,17] in this case enabling single-step production of polymer grade C_2H_4 by removing both C_2H_2 and CO_2 from a ternary C2-CO_2 gas mixture.

Deposition Number 2050185 contains the supplementary crystallographic data for this paper. These data are provided free of charge by the joint Cambridge Crystallographic Data Centre and Fachinformationszentrum Karlsruhe Access Structures service www.ccdc.cam.ac.uk/structures.

Acknowledgements

We thank Dr. Claire Murray and Dr. Chiu C. Tang from the Diamond Light Source, Harwell Science and Innovation Campus, UK for helping us to collect the beamline i11 synchrotron X-ray diffraction data during session EE20500. S.M. acknowledges the Alexander von Humboldt Foundation for postdoctoral research fellowship. M.J.Z. acknowledges the Science Foundation Ireland (awards 13/RP/B2549, 16/IA/4624) and the European Research Council (award ADG 885695). T.P., K.A.F., and B.S. acknowledge the National Science Foundation (Award No. DMR-1607989), including support from the Major Research Instrumentation Program (Award No. CHE-1531590). Computational resources were made available by a XSEDE Grant (No. TG-DMR090028) and by Research Computing at the University of South Florida. For the spectroscopic work, K.T. acknowledges the U.S. Department of Energy, Office of Science, Basic Energy Sciences under Award No. DE-SC0019902. Open access funding provided by IReL.

Conflict of interest

The authors declare no conflict of interest.

Keywords: coordination networks · crystal engineering · ethylene purification · physisorption · porous materials

[1] 2019 Report of The International Council of Chemical Associations, https://icca-chem.org/news/chemical-industry-contributes-5-7-trillion-to-global-gdp-and-supports-120-million-jobs-new-report-shows/, accessed on 26-12-2020 **2019**.
[2] D. S. Sholl, R. P. Lively, *Nature* **2016**, *532*, 435 – 437.
[3] S. Kitagawa, *Angew. Chem. Int. Ed.* **2015**, *54*, 10686 – 10687; *Angew. Chem.* **2015**, *127*, 10834 – 10835.
[4] 2020 Facts and Figures of the European Chemical Industry, https://cefic.org/app/uploads/2019/01/The-European-Chemical-Industry-Facts-And-Figures-2020.pdf, accessed on 26-12-2020 **2020**.
[5] T. Ren, M. Patel, K. Blok, *Energy* **2006**, *31*, 425 – 451.
[6] R. B. Eldridge, *Ind. Eng. Chem. Res.* **1993**, *32*, 2208 – 2212.
[7] B. L. Farrell, V. O. Igenegbai, S. Linic, *ACS Catal.* **2016**, *6*, 4340 – 4346.
[8] M. Oschatz, M. Antonietti, *Energy Environ. Sci.* **2018**, *11*, 57 – 70.
[9] S. Liu, X. Han, Y. Chai, G. Wu, W. Li, J. Li, I. da-Silva, P. Manuel, Y. Cheng, L. L. Daemen, A. J. Ramirez-Cuesta, W. Shi, N. Guan, S. Yang, L. Li, *Angew. Chem. Int. Ed.* **2021**, *60*, 6526 – 6532; *Angew. Chem.* **2021**, *133*, 6600 – 6606.
[10] a) R.-B. Lin, L. Li, H.-L. Zhou, H. Wu, C. He, S. Li, R. Krishna, J. Li, W. Zhou, B. Chen, *Nat. Mater.* **2018**, *17*, 1128 – 1133; b) O. T. Qazvini, R. Babarao, Z.-L. Shi, Y.-B. Zhang, S. G. Telfer, *J. Am. Chem. Soc.* **2019**, *141*, 5014 – 5020; c) O. T. Qazvini, R. Babarao, S. G. Telfer, *Nat. Commun.* **2021**, *12*, 197.
[11] a) S. Mukherjee, D. Sensharma, K.-J. Chen, M. J. Zaworotko, *Chem. Commun.* **2020**, *56*, 10419 – 10441; b) Q. Dong, X. Zhang, S. Liu, R.-B. Lin, Y. Guo, Y. Ma, A. Yonezu, R. Krishna, G. Liu, J. Duan, R. Matsuda, W. Jin, B. Chen, *Angew. Chem. Int. Ed.* **2020**, *59*, 22756 – 22762; *Angew. Chem.* **2020**, *132*, 22944 – 22950.
[12] Z. Bao, G. Chang, H. Xing, R. Krishna, Q. Ren, B. Chen, *Energy Environ. Sci.* **2016**, *9*, 3612 – 3641.
[13] K.-J. Chen, D. G. Madden, S. Mukherjee, T. Pham, K. A. Forrest, A. Kumar, B. Space, J. Kong, Q.-Y. Zhang, M. J. Zaworotko, *Science* **2019**, *366*, 241 – 246.
[14] a) P.-Q. Liao, N.-Y. Huang, W.-X. Zhang, J.-P. Zhang, X.-M. Chen, *Science* **2017**, *356*, 1193 – 1196; b) H.-G. Hao, Y.-F. Zhao,

D.-M. Chen, J.-M. Yu, K. Tan, S. Ma, Y. Chabal, Z.-M. Zhang, J.-M. Dou, Z.-H. Xiao, G. Day, H.-C. Zhou, T.-B. Lu, *Angew. Chem. Int. Ed.* **2018**, *57*, 16067 – 16071; *Angew. Chem.* **2018**, *130*, 16299 – 16303; c) Z. Xu, X. Xiong, J. Xiong, R. Krishna, L. Li, Y. Fan, F. Luo, B. Chen, *Nat. Commun.* **2020**, *11*, 3163.

[15] J. J. Perry IV, J. A. Perman, M. J. Zaworotko, *Chem. Soc. Rev.* **2009**, *38*, 1400 – 1417.

[16] M. Schroeder, *Functional Metal-Organic Frameworks: Gas Storage, Separation and Catalysis*, Springer, Heidelberg, **2010**.

[17] S. Mukherjee, M. J. Zaworotko, *Trends Chem.* **2020**, *2*, 506 – 518.

[18] J.-R. Li, R. J. Kuppler, H.-C. Zhou, *Chem. Soc. Rev.* **2009**, *38*, 1477 – 1504.

[19] a) X. Cui, K. Chen, H. Xing, Q. Yang, R. Krishna, Z. Bao, H. Wu, W. Zhou, X. Dong, Y. Han, B. Li, Q. Ren, M. J. Zaworotko, B. Chen, *Science* **2016**, *353*, 141 – 144; b) B. Li, X. Cui, D. O'Nolan, H.-M. Wen, M. Jiang, R. Krishna, H. Wu, R.-B. Lin, Y.-S. Chen, D. Yuan, H. Xing, W. Zhou, Q. Ren, G. Qian, M. J. Zaworotko, B. Chen, *Adv. Mater.* **2017**, *29*, 1704210.

[20] a) P. Nugent, Y. Belmabkhout, S. D. Burd, A. J. Cairns, R. Luebke, K. Forrest, T. Pham, S. Ma, B. Space, L. Wojtas, M. Eddaoudi, M. J. Zaworotko, *Nature* **2013**, *495*, 80 – 84; b) A. Kumar, D. G. Madden, M. Lusi, K.-J. Chen, E. A. Daniels, T. Curtin, J. J. Perry IV, M. J. Zaworotko, *Angew. Chem. Int. Ed.* **2015**, *54*, 14372 – 14377; *Angew. Chem.* **2015**, *127*, 14580 – 14585; c) P. M. Bhatt, Y. Belmabkhout, A. Cadiau, K. Adil, O. Shekhah, A. Shkurenko, L. J. Barbour, M. Eddaoudi, *J. Am. Chem. Soc.* **2016**, *138*, 9301 – 9307; d) S. Mukherjee, N. Sikdar, D. O'Nolan, D. M. Franz, V. Gascón, A. Kumar, N. Kumar, H. S. Scott, D. G. Madden, P. E. Kruger, B. Space, M. J. Zaworotko, *Sci. Adv.* **2019**, *5*, eaax9171.

[21] H.-M. Wen, L. Li, R.-B. Lin, B. Li, B. Hu, W. Zhou, J. Hu, B. Chen, *J. Mater. Chem. A* **2018**, *6*, 6931 – 6937.

[22] S. P. Thompson, J. E. Parker, J. Marchal, J. Potter, A. Birt, F. Yuan, R. D. Fearn, A. R. Lennie, S. R. Street, C. C. Tang, *J. Synchrotron Radiat.* **2011**, *18*, 637 – 648.

[23] S. K. Elsaidi, M. H. Mohamed, H. T. Schaef, A. Kumar, M. Lusi, T. Pham, K. A. Forrest, B. Space, W. Xu, G. J. Halder, J. Liu, M. J. Zaworotko, P. K. Thallapally, *Chem. Commun.* **2015**, *51*, 15530 – 15533.

[24] K. C. Waterman in *Handbook of Stability Testing in Pharmaceutical Development: Regulations, Methodologies, and Best Practices* (Ed.: K. Huynh-Ba), Springer New York, New York, **2009**, pp. 115 – 135.

[25] A. L. Myers, J. M. Prausnitz, *AIChE J.* **1965**, *11*, 121 – 127.

[26] K.-J. Chen, H. S. Scott, D. G. Madden, T. Pham, A. Kumar, A. Bajpai, M. Lusi, K. A. Forrest, B. Space, J. J. Perry, M. J. Zaworotko, *Chem* **2016**, *1*, 753 – 765.

[27] S. Breda, I. D. Reva, L. Lapinski, M. J. Nowak, R. Fausto, *J. Mol. Struct.* **2006**, *786*, 193 – 206.

[28] C. P. Krap, R. Newby, A. Dhakshinamoorthy, H. García, I. Cebula, T. L. Easun, M. Savage, J. E. Eyley, S. Gao, A. J. Blake, W. Lewis, P. H. Beton, M. R. Warren, D. R. Allan, M. D. Frogley, C. C. Tang, G. Cinque, S. Yang, M. Schröder, *Inorg. Chem.* **2016**, *55*, 1076 – 1088.

[29] A. Kumar, C. Hua, D. G. Madden, D. O'Nolan, K.-J. Chen, L.-A. J. Keane, J. J. Perry, M. J. Zaworotko, *Chem. Commun.* **2017**, *53*, 5946 – 5949.

[30] R. G. Tobin, *Surf. Sci.* **1987**, *183*, 226 – 250.

[31] T. M. McDonald, W. R. Lee, J. A. Mason, B. M. Wiers, C. S. Hong, J. R. Long, *J. Am. Chem. Soc.* **2012**, *134*, 7056 – 7065.

[32] N. B. Colthup, L. H. Daly, S. E. Wiberley, *Introduction to Infrared and Raman Spectroscopy*, 3rd ed., Academic Press, San Diego, **1990**.

[33] K. Nakamoto, *Infrared and Raman Spectra of Inorganic and Coordination Compounds*, 6th ed., Wiley, Hoboken, **2009**.

[34] N. B. Colthup, L. H. Daly, S. E. Wiberley, *Introduction to Infrared and Raman Spectroscopy*, 3rd ed. Academic Press, San Diego, **1990**.

[35] M. Hartmann, S. D. Wetmore, L. Radom, *J. Phys. Chem. A* **2001**, *105*, 4470 – 4479.

[36] O. Shekhah, Y. Belmabkhout, Z. Chen, V. Guillerm, A. Cairns, K. Adil, M. Eddaoudi, *Nat. Commun.* **2014**, *5*, 4228.

[37] H. Wang, Y. Liu, J. Li, *Adv. Mater.* **2020**, *32*, 2002603.

[38] D. P. van Heerden, L. J. Barbour, *Chem. Soc. Rev.* **2021**, *50*, 735 – 749.

[39] Z. Ji, H. Wang, S. Canossa, S. Wuttke, O. M. Yaghi, *Adv. Funct. Mater.* **2020**, *30*, 2000238.

Manuscript received: January 6, 2021
Accepted manuscript online: January 25, 2021
Version of record online: April 1, 2021

